Journal of Biomechanics 85 (2019) 210–217

Contents lists available at ScienceDirect

Journal of Biomechanics

journal homepage: www.elsevier.com/locate/jbiomech
www.JBiomech.com

Short communication

Hemodynamic analysis of a novel stent graft design with slit perforations in thoracic aortic aneurysm

ChiWei Ong [a], Fei Xiong [a], Foad Kabinejadian [b], Gideon Praveen Kumar [c], FangSen Cui [c], Gongfa Chen [d], Pei Ho [e], HwaLiang Leo [a,*]

[a] Department of Biomedical Engineering, National University of Singapore, Singapore
[b] Department of Biomedical Engineering, Tulane University, New Orleans, LA, USA
[c] Institute of High Performance Computing, A*STAR, Singapore 138632, Singapore
[d] Center of Computational Mechanics, Guangdong University of Technology, China
[e] Department of Cardiac, Thoracic & Vascular Surgery, National University Health System, Singapore

ARTICLE INFO

Article history:
Accepted 8 January 2019

Keywords:
Thoracic aortic aneurysm
Computational fluid dynamics
Particle image velocimetry
Flow preservation
Shear stress

ABSTRACT

Thoracic endovascular aortic repair (TEVAR) has been introduced as a less invasive approach to the treatment of thoracic aortic aneurysm (TAA). However, the effectiveness of TEVAR in the treatment of TAA is often limited due to the complex anatomy of aortic arch. Flow preservation at the three supra-aortic branches further increases the overall technical difficulty. This study proposes a novel stent graft design with slit perforations that can positively alter the hemodynamics at the aortic arch while maintaining blood flow to supra-aortic branches. We carried out a computational fluid dynamic (CFD) analysis to evaluate flow characteristics near stented aortic arch in simplified TAA models, followed by *in-vitro* experiments using particle image velocimetry (PIV) in a mock circulatory loop. The hemodynamics result was studied in terms of time-averaged wall shear stress (TAWSS), oscillating shear index (OSI), and endothelial cell action potential (ECAP). The results showed that the stent graft with slit perforations can reduce the disturbed flow region considerably. Furthermore, the effect of the slits on flow preservation to the supra-aortic branches was simulated and compared with experimental results. The effectiveness of the stent graft with slit perforations in preserving flow to the branches was demonstrated by both simulated and experimental results. Low TAWSS and elevated ECAP were observed in the aortic arch aneurysm after the placement of the stent graft with slits, implying the potential of thrombus formation in the aneurysm. On the other hand, the effects of the stent grafts with full-slit design and half-slit design on the shear stress did not differ significantly. The present analysis indicated that not only could the stent graft with slit perforations shield the aneurysm from rupture, but also it resulted in a favorable environment for thrombus that can contribute to the shrinkage of the aneurysm.

1. Introduction

It has been shown that a controlled reduction of velocity can induce systematized thrombus formation which is capable of lessening the wall stress of an aneurysm, protecting it from rupture. Multilayer aneurysm repair system, a multilayer flow modulator (MFM) developed by Cardiatis SA (Isnes, Belgium) has used this concept to treat aortic aneurysms. No embolization was found in all the 24 patients involved in MFM implantation (Oval et al., 2018). Coincidently, Spinella et al. published a midterm follow up of thoracoabdominal aortic aneurysms treated with MFM. No embolization was found in their follow up and their results showed no mortality related to aneurysm rupture even in the high rate of reinterventions after MFM placement (Spinella et al., 2018).

Treatment for aortic aneurysms involving multilayer bare-metal stents has been developed based on the similar concept. A recent systematic review showed that five studies using multilayer bare-metal stent treatment which included 154 patients showed no embolization in patients, 98.4% patency of branch vessels, and almost 0% rupture in aneurysms (Ke et al., 2017). Overlapping stents can also isolate an aneurysm effectively and are believed to create a favorable hemodynamic environment contributing to the degradation of the aneurysm (Zhang et al., 2015; Zhang et al., 2014a). A mid-term cohort study on saccular aneurysms with multiple overlapping uncovered stents demonstrated the significant thrombus deposition speed and shrinkage of the aneurysms.

* Corresponding author.
E-mail address: bielhl@nus.edu.sg (H. Leo).

https://doi.org/10.1016/j.jbiomech.2019.01.019
0021-9290/

Both MFM and multilayer bare-metal stents are still in a clinical study stage and very few reports have discussed them. Similarly, driven by the concept that improved hemodynamics pattern can treat aneurysms, our group developed a stent graft (SG) with slit perforations based on the previous experience in carotid artery bifurcation (Kabinejadian et al, 2016). The blockage of vessel and embolization in vital vessels are very unlikely to happen when thrombus is promoted since such incidences were not observed in the treatment of large aortic aneurysms (thoracic aortic aneurysm and abdominal aortic aneurysm with multiple vital branching arteries) involving MFM and multiple bare-metal stents. We investigated the hemodynamic changes in the vicinity of the stented aortic arch and explored how such changes to SG designs can impact the treatment of TAA.

2. Method

2.1. Geometry

Idealized TAA models were constructed using SOLIDWORKS (Dassault Systèmes SolidWorks Corporation, Waltham, MA) (Fig. 1). The diameter of the aneurysm is approximately 55 mm with the aorta diameter set as 34 mm. The diameters for three

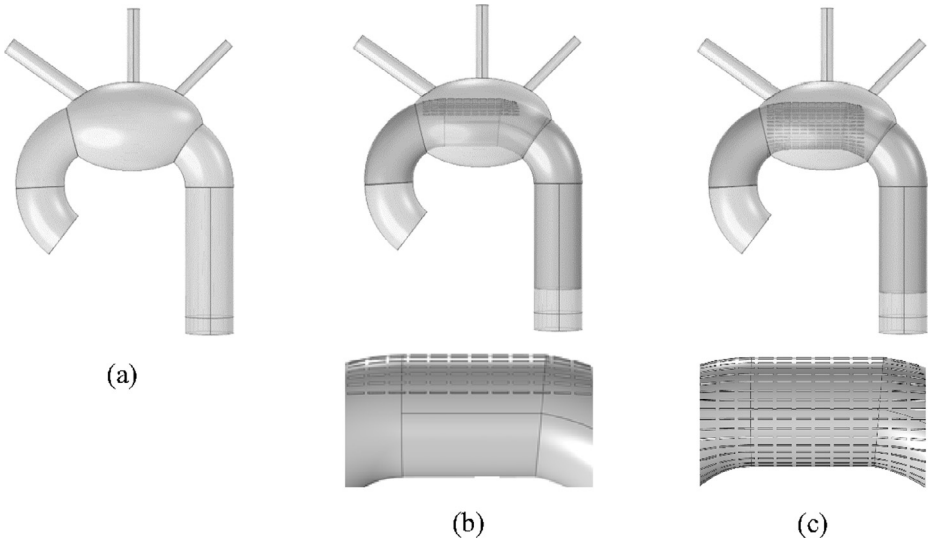

Fig. 1. Idealized aneurysm geometries (a) without SG (b) with half-slit SG (c) with full-slit SG.

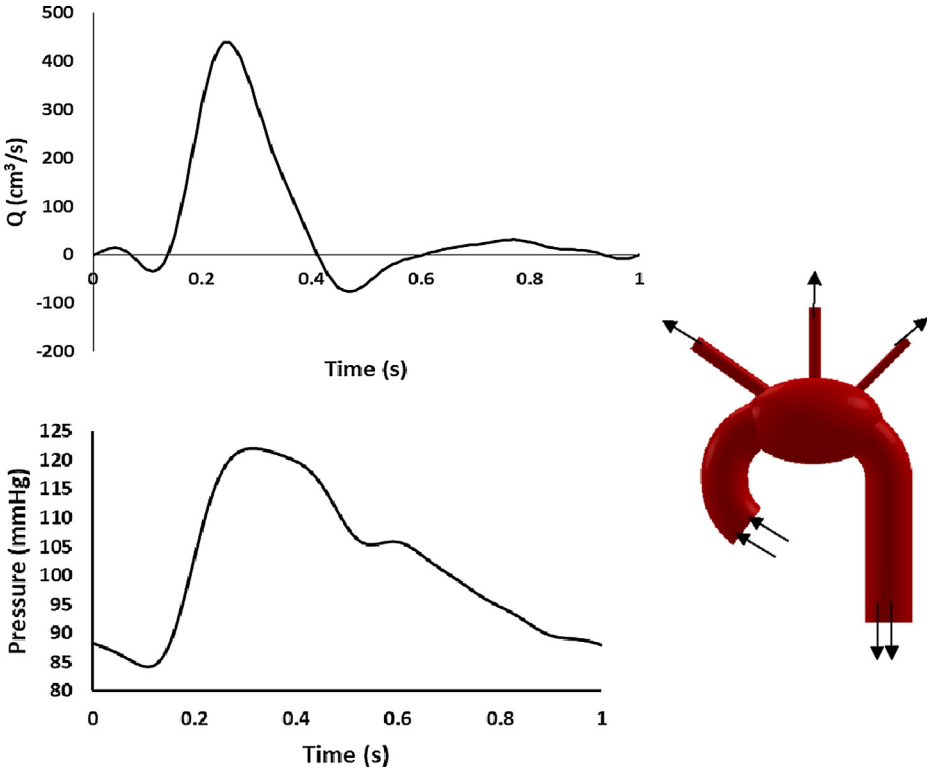

Fig. 2. Time-dependent inlet flow profile and pressure outlet waveforms.

superior branches, namely the brachiocephalic artery (BRA), left common carotid artery (LCA), and left subclavian artery (LSA) are set to 10 mm, 8 mm, and 6 mm, respectively. The SG with full-slit and half-slit designs were virtually implanted in the aneurysm through Boolean algebra in ANSYS workbench (ANSYS Inc., Canonsburg, PA). Full-slit design has slits all over the entire circumference of SG while half-slit design consisted of slits only on the top-half of the SG near the branching section. The half-slit SG is more cost effective than the full-slit counterpart in terms of laser cutting cost. The width and length of the slit segment on the graft is 0.2 mm and 1 mm. As such, the study includes the comparison of hemodynamic characteristics between these two SG designs. All geometries were meshed by ANSYS ICEM with tetrahedral elements.

2.2. Numerical scheme and material properties

CFD simulations were performed using finite volume method in ANSYS FLUENT, where the Navier-Strokes equations for an incompressible flow were solved by iterative Semi-Implicit Method for Pressure Linked Equations (SIMPLE) with a second-order upwind scheme.

Flow continuity equation

$$\nabla \cdot \vec{V} = 0 \tag{1}$$

Flow momentum equation

$$\frac{\partial}{\partial t}\left(\rho \vec{V}\right) + \rho\left(\vec{V} \cdot \nabla\right)\vec{V} = -\nabla p + \rho \vec{g} + \mu \nabla^2 \vec{V} \tag{2}$$

where $\vec{V}$ is the velocity vector described by u, v, w components in x, y, z directions, p, ρ, and μ represent the pressure, density, and viscosity of the fluid.

Blood was modelled as a non-Newtonian fluid using Carreau-Yasuda model (Zhang et al., 2015) to determine blood viscosity. The relationship between shear rate and viscosity is expressed as

$$\eta\dot{\gamma} = \eta + (\eta_0 - \eta_\infty)[1 + (\lambda\dot{\gamma})^2]^{(n-1)/2} \tag{3}$$

where η_∞ and η_0 are the infinite and zero shear rate viscosities, and λ is the relaxation time constant. The model has been found to fit in the experimental data with the following parameters η_∞=3.45 × 10^{-3} kg/(m s), η_0 = 5.6 × 10^{-2} kg/(m s), n = 0.3568 and λ = 3.313 s (Zhang et al., 2015).

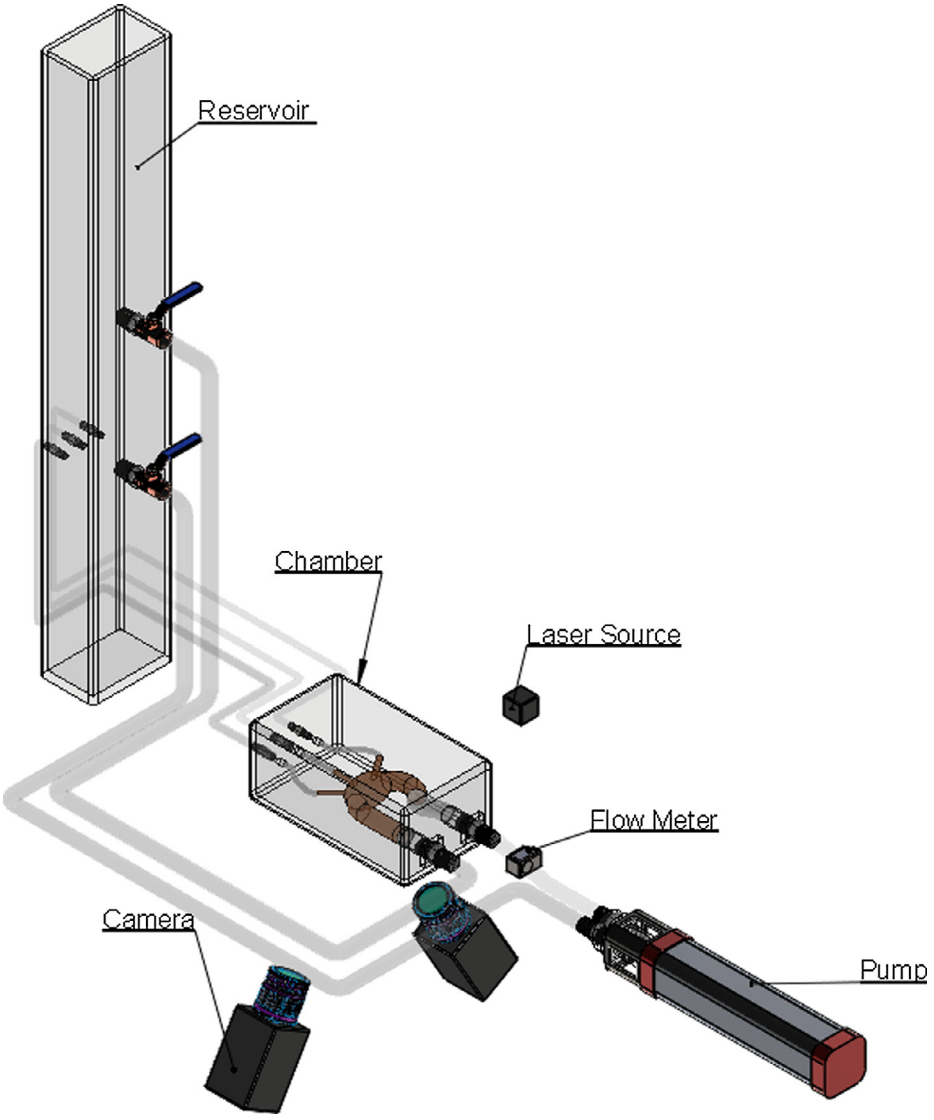

Fig. 3. Mock circulatory loop with 3D PIV setup.

The whole transient simulation was run for five cycles and only the last cycle results are presented. The time step was set as 0.001 s. The convergence residuals were monitored until they reached the convergence criterion of 10^{-5}.

2.3. Boundary conditions

The inlet velocity and outlet pressure waveforms were extracted from the literature (Olufsen et al., 2000) and applied on the model as shown in Fig. 2. The outlet of various branches was prescribed with approximately 5% of the inlet volumetric flow based on the measurements by an ultrasonic flow meter (ME16PXN, Transonic Systems Inc., Ithaca, NY, USA) in the flow loop setup described in Section 2.5. A similar setup has been applied in several published literature (Tse et al., 2011; Shahcheraghi et al., 2002; Shipkowitz et al., 2000). The no-slip condition was applied at the walls.

Mesh sensitivity analysis was conducted with the total number of elements in the models varying from 1.1 million to 2.3 million for the aneurysm without SG implantation, 1.5 million to 3.5 million for the SG with full-slit design, and 1.23 million to 3.1 million for the SG with half-slit design. The difference in the velocity for different mesh size was <2% (Menichini et al 2018, Condemi et al 2018). Therefore, mesh sizes of 1.1 million, 1.5 million, and 1.23 million elements were used for aneurysm, aneurysm with full-slit, and aneurysm with half-slit models, respectively. 10 layers of prismatic elements were formed near the wall to ensure the accuracy of the WSS prediction.

2.4. Quantities of interest

In this work, we studied the time-averaged wall shear stress (TAWSS), oscillatory shear index (OSI), and endothelial cell action potential (ECAP). We also evaluated the site specificity of thrombus distribution in the aneurysm through comparison of different hemodynamic indices.

TAWSS is expressed as the averaged WSS acting upon vessel wall throughout the whole cardiac cycle (Tan et al., 2009),

$$\mathrm{TAWSS} = \frac{1}{T}\int_0^T |\vec{\tau}_w| \tag{4}$$

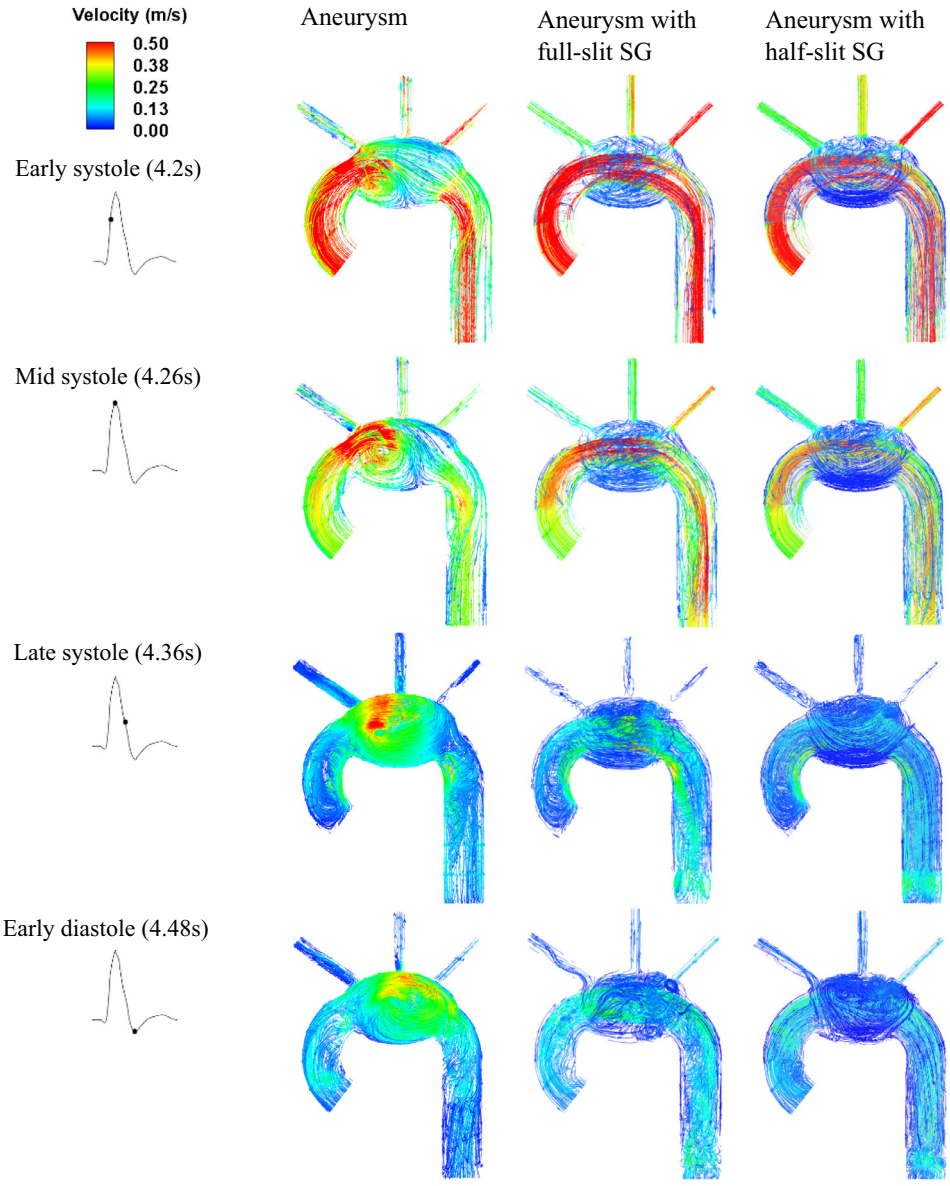

Fig. 4. Flow streamlines in the 3D geometry before and after stent graft implantation.

where $\vec{\tau}_w$ is the WSS vector (traction) and T is the time period of the flow cycle.

OSI (Ku et al., 1985) is used to describe the oscillation of the WSS as defined by

$$\mathrm{OSI} = \frac{1}{2}\left(1 - \frac{\left|\int_0^T \vec{\tau}_w dt\right|}{\int_0^T \left|\vec{\tau}_w\right| dt}\right) \tag{5}$$

where $\vec{\tau}_w$ is the WSS vector, and T is the time period of the flow cycle.

ECAP is the ratio between OSI and TAWSS, which characterizes the degree of 'thrombotic susceptibility' at vessel wall (Kelsey et al., 2017) and is defined as

$$\mathrm{ECAP} = \frac{\mathrm{OSI}}{\mathrm{TAWSS}} \tag{6}$$

2.5. 3D PIV experiment

We set up a mock circulatory system with phantom models similar to that in (Wen et al., 2010) to validate the flow preservation at side branches. The system was driven by a pulse generator (SuperPump AR series, ViVitro Labs Inc., Victoria, BC, Canada) at a flow rate of 5 L/min and a pulse rate of 1 Hz. The reservoir level and mechanical valve were adjusted to mimic the boundary conditions we applied to the computational simulation. The flow rate was measured using two ultrasonic flow meters (ME16PXL & ME10PXN, Transonic Systems Inc., Ithaca, NY, USA). The setup of the entire flow loop is shown in Fig. 3. A 3D PIV system was set up to capture the velocity vectors at the aortic arch. In this experiment, the blood analogue consisted of 40% glycerin and 60% water. Polyamide seeding particles with a mean diameter of 55 μm were added as tracer particles (Kabinejadian et al., 2013). Two CCD

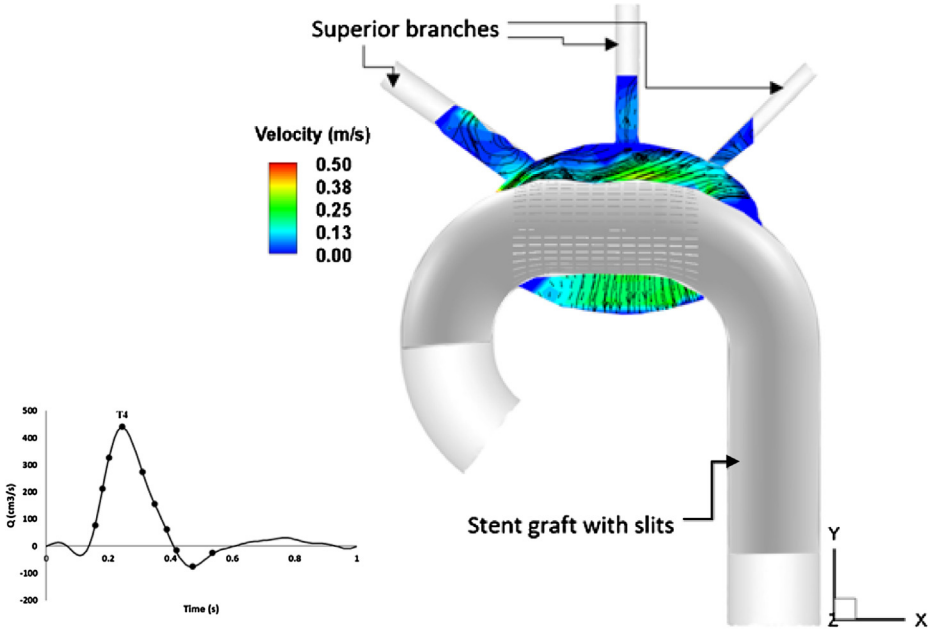

(a)

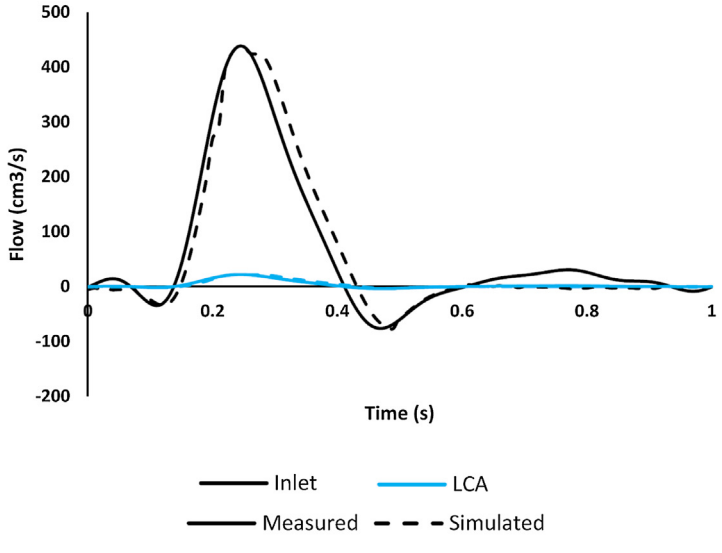

(b)

Fig. 5. (a) The flow velocity field obtained from 3-D PIV in the mid-plane at peak systole (T4). (b) Simulated and measured flow waveform at the inlet and left carotid common artery (LCA).

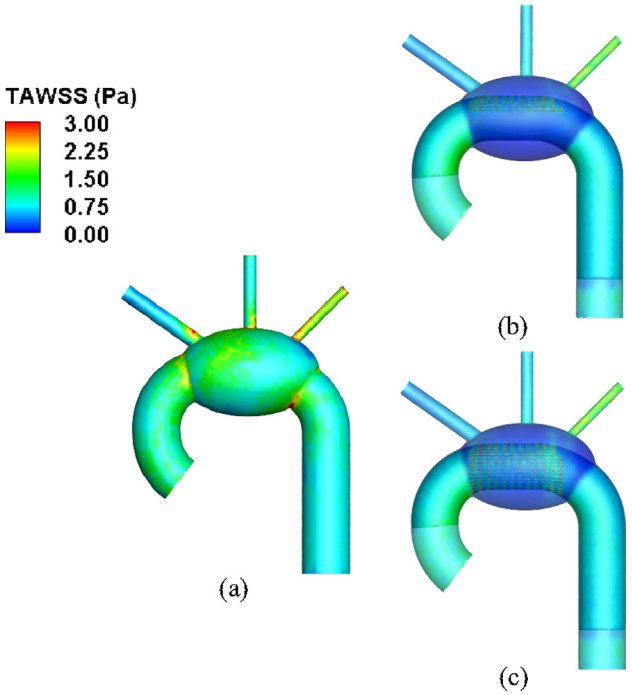

Fig. 6. Contour maps of time-averaged wall shear stress (TAWSS) for the aneurysm (a) without SG, (b) with half-slit SG and (c) with full-slit SG.

(couple-charged device) cameras with a relative angle of 30° were used to generate stereo images. The images were then analyzed by two-frame cross-correlation algorithm with an interrogation area of 64×64 pixels^2 (1924 velocity vectors for an area of about 58×55 mm^2).

3. Results

Fig. 4 illustrates the flow streamlines at four time points in the cardiac cycle for the three aneurysm models: (i) without SG (before the implantation of SG with slits), (ii) with full-slit SG, and (iii) with half-slit SG. Also, we simulated a case of an aneurysm with a bare metal stent as a control. A Zenith stent was implanted in the thoracic aortic aneurysm. The difference in the flow pattern was negligible as compared to the aneurysm model without SG. Hence, we did not include the details in favor of brevity.

For the aneurysm without SG, at early systole, a vortex was formed due to the strong flow impingement on the aneurysmal wall; the vortex gradually shifted to the center of the aneurysm and evolved into a large recirculation at the early diastole. In contrast, no recirculation region was observed in either of the half-slit or full-slit SG models. An isolated low velocity region (<0.1 m/s) was found outside the SG with slits in the aneurysm.

The flow at the superior branches was well maintained as shown in Fig. 5(a), which was further supported by the flow measurement in the mid-plane by PIV at the peak systole. No recirculation was found inside the aneurysm after the implantation of SG. Approximately 5% of the total flow volume was measured at the LCA (Fig. 5(b)). The measured and simulated volumes differ by <5%.

Contours of TAWSS are shown in Fig. 6. In the aneurysm before treatment (without SG) (Fig. 6(a)), the overall TAWSS exceeded 1.50 Pa. After SG implantation, most regions experienced a TAWSS of <0.75 Pa as shown in Fig. 6(b) and (c). Contour plot of OSI is presented in Fig. 7. As shown in Fig. 7(a), large part of the aneurysm was exposed to high OSI (>0.3). Low OSI region (<0.1) was found at the aneurysm after implantation of SG with slits as shown in Fig. 7(b) and (c). Distribution of endothelial cell activation potential (ECAP) is presented in the contour plot in Fig. 8. A low ECAP (<0.35 Pa) was found in the aneurysm model (without SG), as presented in Fig. 8(a). High ECAP (>1.40 Pa) was evident at the entrance to the center of the aneurysm after SG implantation (Fig. 8(b) and (c)).

Shear stress is presented in the line graph as shown in Fig. 9. Both half-slit and full-slit SG demonstrated higher levels of shear stress (>1.50 Pa), whereas low shear stress was found in the aneurysm model before SG implantation. We compared the CFD calculated shear stress and PIV-measured shear stress in the full-slit model, which showed a difference below 15%, validating our computational model.

4. Discussion

The potential of SG with slits in moderating the blood flow in large TAA is still mostly unexplored by today's scientific community. Our results demonstrated that flow interventions by the novel SG with slits can increase the chance of thrombosis within TAA, thereby leading to a protection of aneurysm while preserving decent flow to the side branches.

Our stent graft with slits serves for two purposes. Firstly, it helps to generate thrombus to protect the aneurysm from rupture. Research has shown that systematized thrombosis under low-velocity flow condition can help protect an aneurysm from rupture. Multilayer flow modulator and overlapping stents have utilized this concept to prevent aneurysms from rupture. Second, our stent graft with slits preserves the flow in the side branches to facilities the implantation of second stents to branches which has not been found in other devices. Our results have been confirmed by the

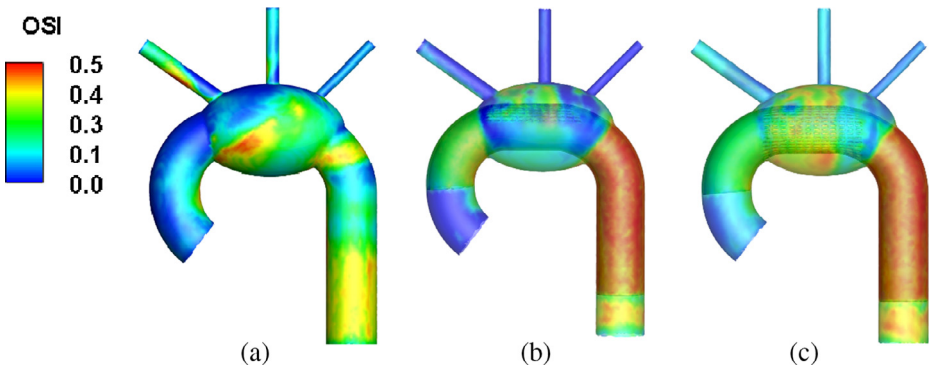

Fig. 7. Contour maps of oscillatory shear index (OSI) for the aneurysm (a) without SG, (b) with half-slit SG and (c) with full-slit SG.

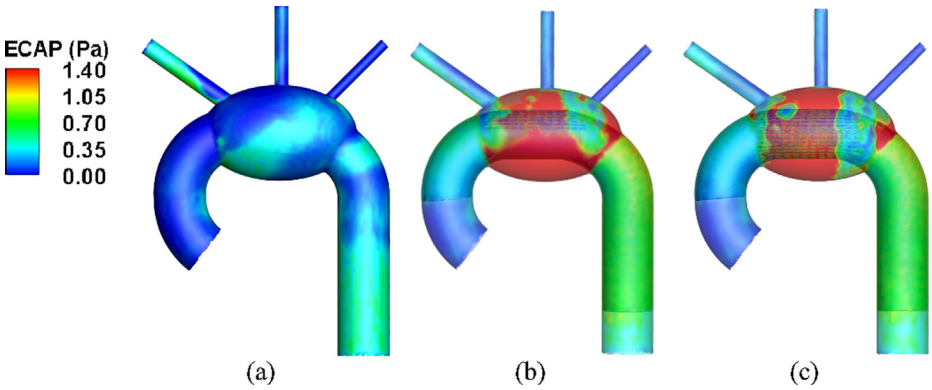

Fig. 8. Contour maps of endothelial cell activation potential (ECAP) for the aneurysm (a) without SG, (b) with half-slit SG and (c) with full-slit SG.

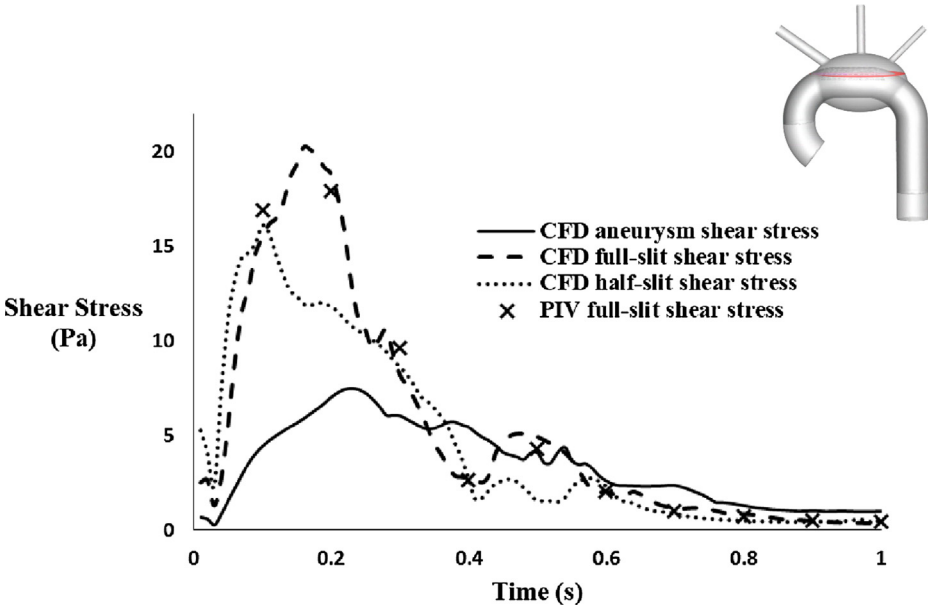

Fig. 9. The maximum shear stress at a cross-sectional plane in the aneurysm over a cardiac cycle for the aneurysm models without SG, with full-slit SG, and with half-slit SG obtained by CFD as well as the PIV calculated shear stress for the full-slit SG model.

flow preservation detected from the particle image velocimetry (PIV) results.

Zhang et al have shown that the TAWSS and OSI reductions observed on the aneurysm wall after overlapping stent placement can create a favorable hemodynamics environment promoting platelet activation and aggregation within aneurysm, which can ultimately lead to degradation of the aneurysm (Zhang et al., 2015; Zhang et al., 2014). In our case, we observed similar hemodynamic changes through our SG with slits. Reduced TAWSS (<0.38 Pa) with low OSI (<0.1) region was observed in the full-slit and half-slit SG models. Several other studies have shown that low TAWSS can promote the adhesion of monocytes (Hardman et al., 2013; Lawrence et al., 1987; Lawrence et al., 1995; Worthen et al., 1987). Low OSI region (<0.1) has been correlated to the formation and growth of thrombus in several studies (Arzani et al., 2017; Arzani et al., 2014). To further corroborate that these hemodynamic changes can lead to thrombus formation, we used the endothelial cell action potential (ECAP) value to relate the hemodynamic changes to thrombus formation within the aneurysm. Di Achille et al. suggested that areas with normalized ECAP values > 5 Pa correlated well with locations of thrombus in AAA patients (Di Achille et al., 2014; Kandail et al., 2016); Kelsey et al. showed that ECAP > 1.4 Pa has a high chance to trigger thrombus formation (Kelsey et al., 2017). Hence in our study, the post-treatment model with SG of either half-slit or full-slit design provides a high chance of thrombus formation.

Shear Stress and transport inside the vessel has also been found to play an important role to regulate the growth of thrombus formation (Sakariassen, 2015; Williams, 2004; Bark, 2013). Shear stress above a certain threshold is sufficient to activate platelets that can lead to thrombosis (Gogia and Neelamegham, 2015; Lee et al., 2016; Miyazaki et al., 1996; Nesbitt et al., 2009). Non-physiological shear stress can activate the von Willebrand factor (vWF) to promote platelet adhesion and aggregation (Tomokiyo,K et al., 2005; Endenbury et al., 1995). Our study suggested that the particles in the half-slit and full-slit models were exposed to higher shear stress (>2 Pa) when compared to the aneurysm without SG. Considering the above observations, we believe SG with slits can trigger thrombosis in the long term.

Limitations. We acknowledge that the non-patient specific blood flow conditions and idealized geometries can cause some differences in the hemodynamics environment. Therefore in the future,

we will consider to simulate a virtual implantation of SG in patient-specific geometries and will perform animal testing to confirm the feasibility of proposed designs.

5. Conclusion

In conclusion, SG with slit perforations can lead to flow isolation in aneurysm with flow preservations at the side branches, as evidenced by the simulated and experimental results. Reduced TAWSS and elevated ECAP indicate that this SG design could create a favorable environment for thrombus formation inside the aneurysm sac. We showed that implantation of our novel SG with slit can be an alternative approach for treatment of TAA with complex anatomies. A safe, totally endovascular, easy to implant and effective SG can be developed based on this concept.

Acknowledgements

This project is financially supported by Singapore Ministry of Education Tier 1 Grant (R-397-000-266-114) and Singapore-China Joint Research Programme (project no. 1610500025). The authors would also like to thank AUN/SEED-Net JICA for providing scholarship to the students.

Conflict of interest

None to declare.

References

Arzani, A., Gambaruto, A.M., Chen, G., Shadden, S.C., 2017. Wall shear stress exposure time: a Lagrangian measure of near-wall stagnation and concentration in cardiovascular flows. Biomech Model Mechanobiol 16, 787–803.

Arzani, A., Suh, G.-Y., Dalman, R.L., Shadden, S.C., 2014. A longitudinal comparison of hemodynamics and intraluminal thrombus deposition in abdominal aortic aneurysms. Am J Physiol Heart Circ Physiol 307, H1786–H1795.

Bark Jr, D.L., Ku, D.N., 2013. Platelet transport rates and binding kinetics at high shear over a thrombus. Biophysical J 105 (2), 502–511.

Condemi, F., Campisi, S., Viallon, M., Croisille, P., Fuzelier, J.F., Avril, S., 2018. Ascending thoracic aorta aneurysm repair induces positive hemodynamic outcomes in a patient with unchanged bicuspid aortic valve. J Biomech 81, 145–148.

Di Achille, P., Tellides, G., Figueroa, C.A., Humphrey, J.D., 2014. A haemodynamic predictor of intraluminal thrombus formation in abdominal aortic aneurysms. Proc Math Phys Eng Sci 470.

Endenburg, S.C., Hantgan, R.R., Lindeboom-Blokzijl, L., Lankhof, H., Jerome, W.G., Lewis, J.C., De Groot, P.G., 1995. On the role of von Willebrand factor in promoting platelet adhesion to fibrin in flowing blood. Blood 86 (11), 4158–4165.

Gogia, S., Neelamegham, S., 2015. Role of fluid shear stress in regulating VWF structure, function and related blood disorders. Biorheology 52, 319–335.

Hardman, D., Doyle, B.J., Semple, S.I., Richards, J.M., Newby, D.E., Easson, W.J., Hoskins, P.R., 2013. On the prediction of monocyte deposition in abdominal aortic aneurysms using computational fluid dynamics. Proc Inst Mech Eng H 227, 1114–1124.

Kabinejadian, F., Cui, F., Zhang, Z., Ho, P., Leo, H.L., 2013. A novel carotid covered stent design: In vitro evaluation of performance and influence on the blood flow regime at the carotid artery bifurcation. Ann Biomed Eng 41, 1990–2002.

Kabinejadian, F., Kaabi Nezhadian, M., Cui, F., Ho, P., Leo, H.L., 2016. Covered stent membrane design for treatment of atheroembolic disease at carotid artery bifurcation and prevention of thromboembolic stroke: an in vitro experimental study. Artif Organs 40 (2), 159–168.

Kandail, H., Hamady, M., Xu, X.Y., 2016. Effect of a flared renal stent on the performance of fenestrated stent-grafts at rest and exercise conditions. J Endovasc Ther 23, 809–820.

Ke, K., Zheng, H., Yang, W., 2017. Is multilayer bare stent safe or effective for the treatment of aortic aneurysms? a meta-analysis with early and mid-term outcomes. Ann Vasc Surg 40, 112–119.

Kelsey, L.J., Powell, J.T., Norman, P.E., Miller, K., Doyle, B.J., 2017. A comparison of hemodynamic metrics and intraluminal thrombus burden in a common iliac artery aneurysm. Int J Numer Method Biomed Eng 33, e2821.

Ku, D.N., Giddens, D.P., Zarins, C.K., Glagov, S., 1985. Pulsatile flow and atherosclerosis in the human carotid bifurcation. Positive correlation between plaque location. Arter. Thromb. Vasc. Biol. 5 (3), 293–302.

Lawrence, M., McIntire, L., Eskin, S., 1987. Effect of flow on polymorphonuclear leukocyte/endothelial cell adhesion. Blood 70, 1284–1290.

Lawrence, M.B., Berg, E.L., Butcher, E.C., Springer, T.A., 1995. Rolling of lymphocytes and neutrophils on peripheral node addressin and subsequent arrest on ICAM-1 in shear flow. Eur J Immunol 25, 1025–1031.

Lee, H., Kim, G., Lim, C., Lee, B., Shin, S., 2016. A simple method for activating the platelets used in microfluidic platelet aggregation tests: Stirring-induced platelet activation. Biomicrofluidics 10, 064118.

Menichini, C., Cheng, Z., Gibbs, R.G., Xu, X.Y., 2018. A computational model for false lumen thrombosis in type B aortic dissection following thoracic endovascular repair. J Biomech 66, 36–43.

Miyazaki, Y., Nomura, S., Miyake, T., Kagawa, H., Kitada, C., Taniguchi, H., Komiyama, Y., Fujimura, Y., Ikeda, Y., Fukuhara, S., 1996. High shear stress can initiate both platelet aggregation and shedding of procoagulant containing microparticles. Blood 88, 3456–3464.

Nesbitt, W.S., Westein, E., Tovar-Lopez, F.J., Tolouei, E., Mitchell, A., Fu, J., Carberry, J., Fouras, A., Jackson, S.P., 2009. A shear gradient–dependent platelet aggregation mechanism drives thrombus formation. Nat Med 15, 665.

Olufsen, M.S., Peskin, C.S., Kim, W.Y., Pedersen, E.M., Nadim, A., Larsen, J., 2000. Numerical simulation and experimental validation of blood flow in arteries with structured-tree outflow conditions. Ann Biomed Eng 28, 1281–1299.

Oval, C., Sahin, A., Eroglu, M., Balcin, S., Dernek, S., Sevin Mustafa, B., 2018. Treatment of aortic and iliac artery aneurysms with multilayer flow modulator: single centre experiences. Int J Vasc Med, 9.

Sakariassen, K.S., Orning, L., Turitto, V.T., 2015. The impact of blood shear rate on arterial thrombus formation. Future Sci OA 1 (4), FSO30. https://doi.org/10.4155/fso.15.28.

Shahcheraghi, N., Dwyer, H.A., Cheer, A.Y., Barakat, A.I., Rutaganira, T., 2002. Unsteady and three-dimensional simulation of blood flow in the human aortic arch. J Biomech Eng 124, 378–387.

Shipkowitz, T., Rodgers, V.G.J., Frazin, L.J., Chandran, K.B., 2000. Numerical study on the effect of secondary flow in the human aorta on local shear stresses in abdominal aortic branches. J Biomech 33, 717–728.

Spinella, G., Finotello, A., Faggiano, E., Pane, B., Conti, M., Gazzola, V., Auricchio, F., Palombo, D., 2018. Midterm follow-up geometrical analysis of thoracoabdominal aortic aneurysms treated with multilayer flow modulator. Ann Vasc Surg 53, 97–104.e102.

Tan, F., Torii, R., Borghi, A., Mohiaddin, R., Wood, N., Xu, X., 2009. Fluid-structure interaction analysis of wall stress and flow patterns in a thoracic aortic aneurysm. Int. J. Appl. Mech 1, 179–199.

Tomokiyo, K., Kamikubo, Y., Hanada, T., Araki, T., Nakatomi, Y., Ogata, Y., Moroi, M., 2005. Von Willebrand factor accelerates platelet adhesion and thrombus formation on a collagen surface in platelet-reduced blood under flow conditions. Blood 105 (3), 1078–1084.

Tse, K.M., Chiu, P., Lee, H.P., Ho, P., 2011. Investigation of hemodynamics in the development of dissecting aneurysm within patient-specific dissecting aneurismal aortas using computational fluid dynamics (CFD) simulations. J Biomech 44 (5), 827–836.

Wen, C.-Y., Yang, A.-S., Tseng, L.-Y., Chai, J.-W., 2010. Investigation of pulsatile flowfield in healthy thoracic aorta models. Ann Biomed Eng 38, 391–402.

Williams, R.H., Nollert, M.U., 2004. Platelet-derived NO slows thrombus growth on a collagen type III surface. Thrombosis journal 2 (1), 11.

Worthen, G., Smedly, L., Tonnesen, M., Ellis, D., Voelkel, N., Reeves, J., Henson, P., 1987. Effects of shear stress on adhesive interaction between neutrophils and cultured endothelial cells. J Appl Physiol 63, 2031–2041.

Zhang, P., Liu, X., Sun, A., Fan, Y., Deng, X., 2015. Hemodynamic insight into overlapping bare-metal stents strategy in the treatment of aortic aneurysm. J Biomech 48, 2041–2046.

Zhang, P., Sun, A., Zhan, F., Luan, J., Deng, X., 2014a. Hemodynamic study of overlapping bare-metal stents intervention to aortic aneurysm. J Biomech 47, 3524–3530.

Zhang, Y., Teng, Z., Lu, Q., Zhao, Z., Bao, J., Feng, X., Feng, R., Chen, Z., Huang, Y., Sadat, U., Gillard, J.H., Jing, Z., 2014b. Management of complicated aortic aneurysms using multiple overlapping uncovered stents: mid-term outcome from a cohort study. Medicine 93. e209 e209.